*33rd EPS Conference on Plasma Phys. Rome, 19 - 23 June 2006 ECA Vol.**30I**, P-5.089 (2006)*

Electron temperature profiles and local energy transport in RFX-mod

A. Alfier[1,2], R. Pasqualotto[1], F. Auriemma[1], F. Bonomo[1,2], A. Fassina[1], P. Franz[1], M. Gobbin[1,2], P. Innocente[1], P. Martin[1,2], L. Marrelli[1], P. Piovesan[1], G. Spizzo[1]

[1] *Consorzio RFX – Euratom/ENEA Association – Padova, Italy*

[2] *University of Padova, Department of Physics – Padova, Italy*

1. Introduction

Aiming at a more resolved and accurate measurement of the T_e profile, the Thomson scattering (TS) diagnostic has recently undergone an extensive upgrade, and it has been routinely operational since the beginning of 2005 when the modified RFX experiment (RFX-mod) restarted its operation. RFX-mod (r=0.459m, R=2m) has a passive conductive shell thinner than the old RFX (3mm thick instead of 65mm), but this is compensated by a set of 4 (poloidally distributed) x 48 (toroidally) saddle coils with independent power supplies, that allow to actively control the magneto-hydro-dynamic (MHD) modes, like cancelling the local B_r (Virtual Shell, VS [1]). This paper presents a description of the new TS diagnostic, illustrates the T_e profiles measured during the first experimental campaigns of RFX-mod, showing how VS mode allows to achieve higher T_e, suggesting an improvement in the thermal transport properties of electrons [2].

2. The main Thomson scattering diagnostic on RFX-mod

Only the geometry and the mechanical structure of the old TS system have been retained [3]. The most significant modification is the replacement of the grating spectrometers by a set of 4-filter polychromators with avalanche photodiodes (APDs), which improves the sensitivity by a factor of about 50 using the same ruby laser as input source. More resolved profiles with 84 points and 10 mm resolution (–0.96 to 0.84 r/a) are now being measured with 28 polychromators employing optical delay lines. As the APDs are compatible with Neodymium lasers, the ruby laser has been replaced by a Nd:YLF laser that can produce a burst of 10 pulses at 50Hz during a plasma discharge of 300 ms. Finally the data acquisition system is not any more gating-based, but the full time trace is recorded by means of waveform digitizers. Moreover, the relative calibration of spectral channels has been performed with a Supercontinuuum pulsed white Light Source (SLS) [4] and n_e profiles have been measured using the absolute calibration of the system with Rotational Raman Scattering in Nitrogen.

3. T_e profiles properties

The more evident consequence of the active control system is the longer lasting discharge, from ~100ms to ~300ms, that allows to fully exploit the burst of 10 laser pulses of the TS

diagnostic. As far as plasma thermal properties are concerned, available profiles are mostly obtained at 500kA<I_p<700kA; this doesn't allow to present a complete comparison of electron core temperature during SD (standard discharges), VS and RFX discharges, and confers more uncertainty to low current results. In particular, standard discharges (SD) at $I_p \geq 600$kA are not easily performed, because stronger plasma-wall interactions have been observed in RFX-mod, as a consequence of the thinner passive conductive shell. In fig.1, average core electron temperature $T_e(0)$ is shown as a function of I_p. In VS mode $T_e(0)$ is higher by about 30% than in SD. In SD $T_e(0)$ is smaller than in RFX in similar plasma condition, while in VS $T_e(0)$ is higher. A dependence of the scaling $T_e(0)$ vs. I_p from I/N has not clearly been found, differently from what evidenced in RFX [5].

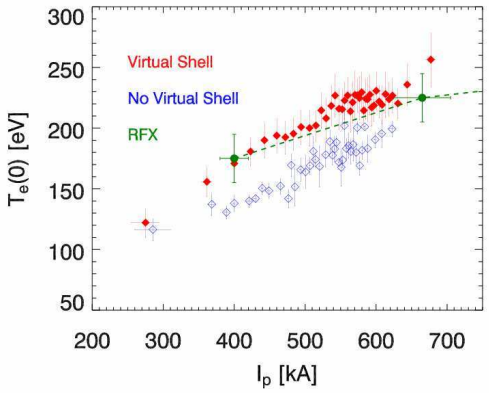

Fig. 1: $T_e(0)$ vs I_p, at I/N ~[$3e^{-14}$ – $5e^{-14}$]Am for Ip<700kA, during VS, SD and respect to RFX [5].

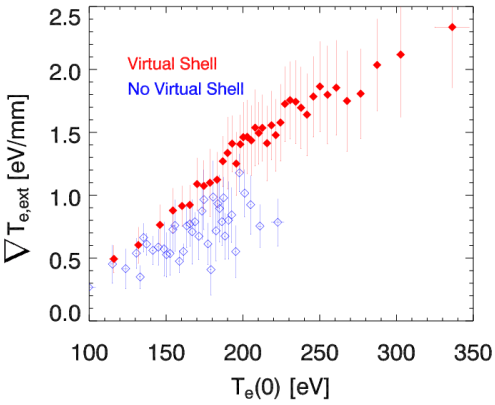

Fig. 2: $\nabla T_{e,ext}$ vs Te(0), at I/N~[$3e^{-14}$ – $5e^{-14}$] Am for Ip<700kA, during VS and SD

Active mode control provides a remarkable suppression of radial magnetic fluctuation [6], reducing the plasma-wall interaction and allowing a better control of electron density and accessibility to higher I/N values. Te is always higher for all I/N values. With the active control system, improved plasma thermal properties are also revealed by the appearing of

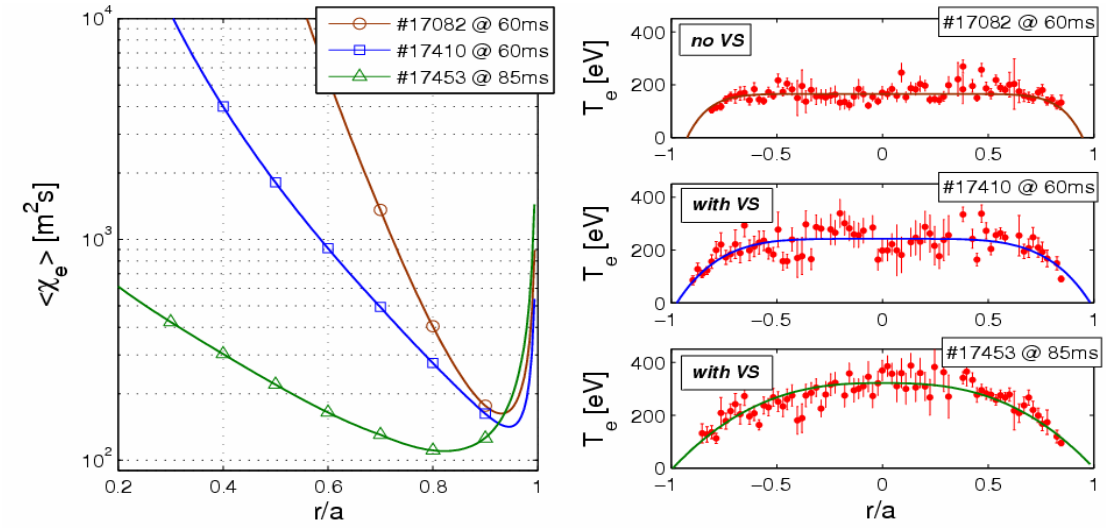

Fig.3: χ_{eff} and corresponding Te profiles in three representative profiles, in SD (brown), VS (blue) and an optimum case (green).

higher temperature gradient in the edge region, $\nabla T_{e,ext}$, from 1eV/mm to 2eV/mm (see fig.2), and obtained by a linear fit of measuring points in r/a > 0.7.

3. Heat conductivity

Steeper edge gradients are indicative of a decrease of electron heat transport during VS. An estimate of such a reduction has been obtained by applying the 1D steady state power balance equation [5],[7]. Adopting a single fluid approach, the effective thermal conductivity has been deduced as $\chi_{eff} = -q_{\perp}(r)/[n_e(r)\cdot\nabla T_e(r)]$. The energy flux has been evaluated integrating the expression $\nabla\cdot q_{\perp}(r)= \Omega(r) - \varepsilon(r)$, where $\Omega(r) = E(r)\cdot j(r)$ is the ohmic power deposition profile, and $\varepsilon(r)$ is the experimental total radiation emissivity, mostly localized in the plasma edge and typically from 5% to 20% of the input power. The current density $j(r)$ profile is reconstructed from external magnetic measurements with the μ&p-model [8]. $E(r)$ is modelled through a local Ohm's law with Spitzer resistivity, where the effective charge is assumed uniform over the line integral of a line-free visible continuous emission.

In fig.3 we report three representative profiles. During SD (brown profiles), heat diffusivity profile has its minimum value, typically 150÷200m^2s, normally at r/a~0.95. Moving inward, it rapidly increases, as a consequence of the flat temperature profile in the core. This is consistent with a poorly confined plasma core where a large region of stochastic magnetic field is likely present, produced by dynamo fluctuations. Active reduction of B_r during VS (blue profiles) decreases the field stochasticity in the core, with the effect of slightly reducing the minimum value of χ_{eff} by about 20% and being distributed in a wider region r/a~[0.90–0.95]. Interestingly, the main effect is in the inner region, r/a~[0.5-0.7], where the temperature gradient is still appreciably non-zero, and the average χ_{eff} is about 5 times lower than in SD. This is supported by the statistical dependence of χ_{eff} in this region as a function of core temperature (fig.4) which also shows that local electron confinement improves at higher T_e.

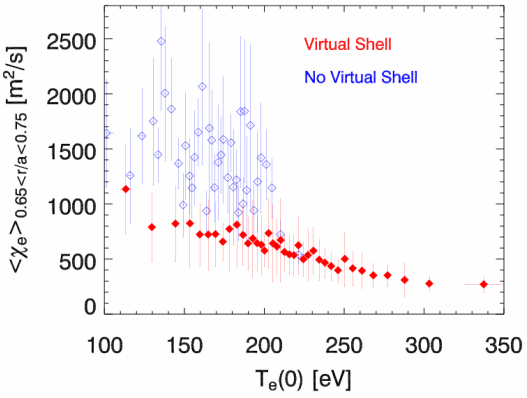

Fig.4: χ_{eff} averaged in r/a~[0.65-0.75] respect to core electron temperature

Better performances have been obtained in the third case (green profile in fig.3): it is characterised by very low mode amplitudes with a n=-7 dominant mode (see black line in fig.5.a). Despite the low fluctuation amplitude at the edge, the $n=-7$ eigenfunction,

reconstructed via Newcomb's equations [9], is large in the core. In RFX-mod the n=-7 mode is the innermost resonant; in the core region the *q* profile is rather flat and even a small perturbation can produce a large island, originating significant temperature gradients, despite the lower edge fluctuation amplitude (fig.5.a). This causes an increased electron temperature and the formation of significant and asymmetric temperature gradients in the core region reported in fig 3. The presence of the helical structure has been confirmed by the SXR tomography [10] (fig.6), and predicted by simulations through guiding centre codes [11].

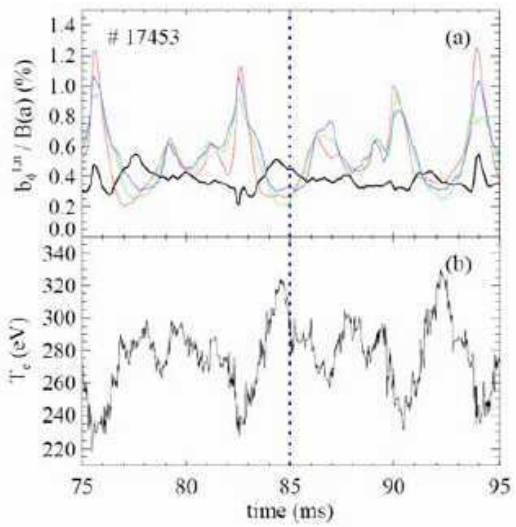

Fig.5: time evolution of selected m=1 modes amplitude and (b) core electron temperature for #17453.

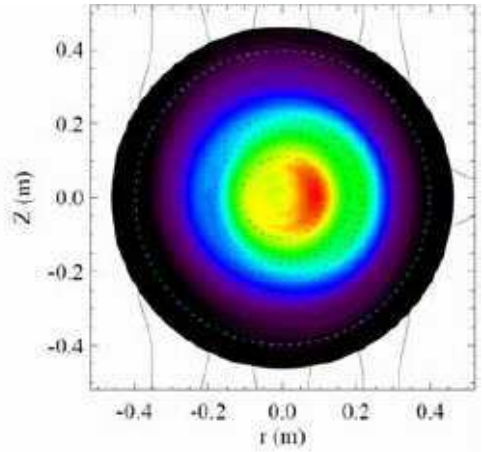

Fig.6: SXR emissivity distribution for #17453 at t=84.57ms. The n=-7 island is shown.

We observe a further reduction of χ_{eff} by a factor 10 in the inner region due to the decrease of magnetic chaos; its minimum is more flattened, shifted inward and reduced to χ_{eff} ~100m^{2}s. As expected from this analysis of χ_{eff}, also the electron confinement time is accordingly enhanced in VS [2]. A more accurate analysis will be executed computing a 2D model that better describes the helical structure.

Acknowledgement*. This work was supported by the European Communities under the contract of Association between EURATOM/ENEA. The views and opinions expressed herein do not necessarily reflect those of the European Commission. This work was partly supported by the Swiss National Science Foundation.*

[1] P. Sonato et al., Fusion Engineering and Design, **66**, 161 (2003).
[2] L. Carraro, this conference (P5.084).
[3] R. Pasqualotto et al., Rev. Sci. Instrum. 72, 1134 (2001).
[4] R. Pasqualotto, A. Alfier, accepted for publication on Rev. Sci. Instrum.
[5] R. Bartiromo et al., Phys. Plasmas 6, 1830 (1999).
[6] S. Ortolani, this conference (I4.005).
[7] R. Pasqualotto et al., 27th EPS, (Montreux, Swiss, 1999).
[8] S. Ortolani and D.D. Schnack, *Magnetohydrodynamics of Plasma Relaxations* (World Scientific, Singapore, 1993).
[9] D.C. Robinson Nucl. Fusion 18, 939 (1978).
[10] P. Franz et al., Nucl. Fusion 41, no 6, 695 (2001).
[11] M. Gobbin, this conference (P1.188).